Numerical modelling of water infiltration into the three components of porosity of a vertisol from Guadeloupe

Stephane Ruy, Liliana Di Pietro, Yves-Marie Cabidoche

1 **Numerical modelling of water infiltration into the three components of**

2 **porosity of a Vertisol from Guadeloupe.**

3 S. RUY[a, *], L. DI PIETRO[a], and Y.M. CABIDOCHE[b]

4 [a] *INRA, Unité de Science du Sol, Domaine St Paul, Agroparc, 84914 Avignon Cedex 9, France*

5 [b] *INRA, Unité Agropédoclimatique de la Zone Caraïbe, B.P. 515, 97165 Pointe à Pitre Cedex, Guadeloupe,*

6 *French West Indies*

7 **Abstract**

8 We present a mechanistic model of soil deformation and water infiltration into a Vertisol of

9 Guadeloupe (French West Indies), which accounts for the three components of porosity of this

10 soil (matric, structural and macro-cracks). Time and space scales are respectively of several

11 hours and the prism delimited by macro-cracks. The model accounts for water movements

12 from the structural porosity and from the macro-cracks into the matric porosity. It simulates

13 the non-equidimensional deformations of the prism resulting from water storage in the matric

14 porosity. Inputs of the model, measured in the laboratory, are the shrinkage curve, the

15 retention curve and the hydraulic conductivity of the matric porosity. The anisotropy ratio of

16 the soil deformation was measured *in situ*. Experiments were conducted *in situ* to provide

17 structural parameters and data to fit and test the model. It is possible to find a unique set of

18 parameters for each experiment. However, parameters significantly differ from one

19 experiment to another. The model shows that the structural water flow regulates the partition

20 of water infiltrating within the prism and of water flowing in the macro-cracks. The model

21 does not accurately predict water infiltration because of a poor modelling of water flow in the

22 structural porosity.

23 **Keywords**

24 swelling clay soil, vertisol, crack, macroporosity, Guadeloupe, infiltration, preferential flow.

1- Introduction

Water flow in heavy clay soils is dominated by macropore flow. Darcy's law describes water flow in small pores (micropores), whereas this law does not apply to water movement within macropores in which gravity is the main driving force (Beven & Germann, 1982). Most models predicting water infiltration into macroporous soils are based on the concept of a bimodal porosity (Hoogmoed & Bouma, 1980; Beven & Germann, 1981; Jarvis & Leeds-Harrison, 1987; Chen & Wagenet, 1992; Jarvis 1994). None of these models apply to a Vertisol because the total porosity of Vertisols can not be reduced to a bimodal porosity. Furthermore these models are one-dimensional and the deformation of the soil is not or poorly accounted for. Garnier *et al*. (1997) proposed a numerical model of 3-dimensional anisotropic deformation and water flow in a swelling clay paste without macropores. Bronswijk (1988) proposed a general procedure to incorporate macro-crack opening and closure into simulation models of water infiltration in clay soils by introducing the shrinkage curve and a geometry factor of anisotropy, r_s.

A model of infiltration and soil deformation in a Vertisol should account for three porosity compartments (Cabidoche & Ozier-Lafontaine, 1995; Ruy, 1997): macro-cracks delimiting continuous soil prisms, intra-prism structural porosity and matric porosity. The almost vertical macro-cracks, several decimetres apart, open and close as the clay particles reorganise in response to soil moisture changes. Their width ranges from 0 for a saturated soil to several cm at the end of the dry season. Water entering these cracks may infiltrate laterally into the walls of the soil matrix. The matric porosity is formed by the arrangement of clay particles. Matric pores are less than about 5 µm in width (Wilding & Tessier, 1988). They remain saturated during structural and normal shrinkage (as defined by Stirk, 1954) and thus contains the water responsible for soil movement. The limit between structural and normal shrinkage is called

---

* Corresponding author. Email : ruy@avignon.inra.fr

1   the crack air entry (CAE) point. The intra-prism structural porosity has a relatively stable

2   geometry (Cabidoche & Ozier-Lafontaine, 1995). Structural pores are from about 10 µm to

3   several mm in width (Yule & Ritchie, 1980; Ruy, 1997). Structural water does not induce any

4   deformation of the soil (Yule & Ritchie, 1980). Shrinkage cracks are not included in structural

5   porosity.

6   In order to better understanding the processes of water infiltration in an undisturbed swelling

7   clay soil, we present the physical bases of a 2D numerical model of water infiltration and soil

8   movements in a Vertisol. Calibration and validation results are also discussed.

9   **2- Physical bases and description of the model**

10   The model is 2D, the scale of modelling is a half prism isolated by one macro-crack. The

11   experimental size of a prism can be deduced from the network of macro-cracks. The variation

12   of the macro-crack aperture with depth can be calculated from measurements of the anisotropy

13   ratio and variations of soil layer thicknesses.

14   *(i) water flow in the matric porosity*

15   We assume that water flow is described by Darcy's law because of the small diameter and the

16   homogeneous distribution of the size of the matric pores (Ruy, 1997). 2D Richard's equation

17   is used to calculate water fluxes. A source function S_w accounts for the diffusive water

18   movement from structural porosity to matric porosity, as suggested by Jarvis (1994):

$$S_w = K_{w/s}\left(\psi_{mat}\right) \cdot S_{struc} \cdot \frac{\psi_{struc} - \psi_{mat}}{d^2} \quad , \qquad (1)$$

19   where $K_{w/s}$ (cm s^{-1}) is the matric conductivity, ψ_{mat} (cm) the potential of water in matric

20   porosity, ψ_{struc} (cm) the potential of water in structural porosity, S_{struc} the saturation of

21   structural porosity and d (cm) an effective "diffusion" length. We suppose that the potential of

22   water in the structural porosity is a linear function of the saturation of this porosity: ψ_{struc} is

23   equal to 0 cm when the structural porosity is saturated and is equal to ψ_{ae} when it is air filled,

1   where ψ_{ae} is the soil water potential at the CAE point (Ruy, 1997). The overburden

2   component of the total potential of water (Philip, 1969) is not accounted for (Ruy &

3   Cabidoche, 1998).

4   We used the finite element method to discretize the domain with rectangular elements. The

5   boundary condition at the surface is a Neumann's condition according to *(iv)*. A zero flux

6   condition is imposed at the bottom of the profile and along the vertical axis of the soil prism,

7   because of the symmetry of the soil prism. The boundary condition along the macro-crack

8   wall is a function of the depth of ponded water in the crack and is described in subsection *(iii)*.

9   *(ii) water flow in the intra-prism structural porosity*

10   We measured continuously in the field the variations of water content (WC) with depth and

11   time for several weeks in previous experiments that are detailed in Ruy (1997). We observed

12   an increase of the structural WC when the matric WC was constant. Macro-cracks were not

13   sampled. These results showed that water flow inside the prism could not be modelled by

14   Darcy's law with a bimodal hydraulic conductivity and water retention curve, and therefore

15   that water flow inside the structural porosity was of "preferential flow type". Then ,we assume

16   that water flow in the structural porosity is a gravity flow.

17   The soil profile is divided into 7 layers, 20 cm in height (except the surface layer whose height

18   is only 10 cm). Water flow is described in a conceptual way by using a model of reservoirs in

19   cascade (one reservoir per layer). For each layer, the volume of the reservoir is the volume of

20   the structural porosity. The output flux q of each reservoir (Figure 1) is a power function of

21   the saturation of the reservoir:

$$q = c \cdot S_{struc}^{b} \quad , \tag{2}$$

22   where c (cm s^{-1}) is the unknown hydraulic conductance, S_{struc} the saturation of the reservoir

23   (*i.e.* the saturation of the structural porosity) and b an empirical exponent. Beven & Germann

24   (1981) and Jarvis & Leeds-Harrison (1987) used a similar power law function for relating

4

1   water flow in macropores and water content. Theoretical values of b can be calculated from

2   the laminar film flow theory in a single, smooth and vertical macropore. For open channel

3   flow, a power law function similar at eq. (2) relates the flow and the depth of water (e.g.

4   Maheshwari, 1994): the exponent ranges from 3 (laminar flow) to 5/3 (turbulent flow and

5   Manning-Strickler relation) or 2/3 (turbulent flow and Chezy relation) (Chen & Wagenet,

6   1992). In our case, no experimental study was available to conclude on the type of flow in the

7   structural porosity. The flow is assumed to be turbulent, and we set the value of b to 1.5.

8   A mass balance is performed at each time step and for every layer between the input flux

9   (which is the output flux of the layer above), the output flux, the volume of water that

10   infiltrates into the matric porosity (the S_w function, see eq. (1)), and the accumulation of water.

11   The bottom of the profile is impervious.

12   *(iii) water flow into the macro-cracks*

13   Ruy (1997) showed that overland flow on a drained parcel of Vertisol was intercepted by

14   macro-cracks and was then rapidly removed by drain pipes before infiltrating horizontally into

15   the prisms. It was however impossible to quantify this process. For a heavy clay soil in the

16   Netherlands (Typic Fluvaquents), Hoogmoed & Bouma (1980) showed that horizontal

17   absorption of water into the prism represents only a small percentage of the volume of water

18   by-passing in the cracks. Moreover, numerical simulations conducted by Di Pietro (1996) on

19   an artificial medium showed that the front velocity of water infiltration within a crack

20   increases with an increasing crack aperture and a decreasing hydraulic conductivity of the

21   matric porosity. This results in a decreasing amount of water horizontally entering into the

22   matric porosity. However, in the absence of drains or when macro-cracks close above drain

23   pipes, free water may accumulate at the bottom of macro-cracks where it can be slowly

24   absorbed into the prisms (Jaillard & Cabidoche, 1984).

25   In the model, water infiltrating into the macro-crack instantaneously reaches the bottom of the

1 crack where it accumulates. Horizontal infiltration into the soil prism during downward

2 unsaturated flow along the macro-crack wall is neglected, whereas it is taken into account for

3 ponded conditions at the bottom of the macro-crack. Hence, the lateral boundary condition for

4 the resolution of the 2D Richard equation is a zero flux condition above the surface of the

5 ponded water, and a Dirichlet condition below this surface (hydrostatic profile). At each time

6 step, the model recalculates the volume of the macro-crack and the depth of the surface of the

7 ponded water according to a mass balance and to the deformation of the soil matrix.

8 *(iv) partitioning of rainfall at the soil surface (Table 1)*

9 First, rainfall, R, enters the matric porosity as long as its intensity does not exceed the

10 infiltrability of the matrix, $I_{\mathrm{mat}}^{\max}$. Then, excess water flows into the structural porosity and then

11 into the macro-cracks if rainfall intensity exceeds the infiltration capacity of both matric and

12 structural porosities, $I_{\mathrm{mat}}^{\max} + I_{\mathrm{struc}}^{\max}$. If the macro-crack is filled with water or closed at the surface,

13 its infiltrability, $I_{\mathrm{crac}}^{\max}$, is nil and any excess water is lost as instantaneous surface runoff.

14 Matric (resp. structural) infiltrability is computed from a mass balance performed on the first

15 layer of finite elements, see subsection *(i)* (resp. first reservoir, see subsection *(ii)*).

16 *(v) deformation of the soil matrix*

17 Clay particles reorganise as water infiltrates into matric porosity, and the soil prism is

18 deformed in every directions according to the anisotropy ratio of soil movements. Swelling is

19 supposed to be normal, *i.e.* any entrance of water results in an equal increase of the bulk

20 volume. We used in the model the anisotropy ratio k of Voltz & Cabidoche (1995): k is the

21 elongation rate in any horizontal direction divided by the elongation rate in the vertical

22 direction. It ranges from 0 (1D vertical swelling) to 1 (equidimensional deformation) and

23 $k \rightarrow \infty$ for horizontal movements only. The model deforms each finite element at each time

24 step according to the variation of the mean matric WC of the element.

1   Table 2 presents a synthesis of all the equations used in the numerical model.

2   *(vi) Numerical considerations.*

3   We chose to make the calculations separately with respect to the flow domains. 2D water

4   infiltration in the matric porosity domain is first calculated. Vertical and horizontal boundary

5   conditions are calculated and Richards' equation is then linearised and solved by an implicit

6   method (Euler's method). The initial time step is 30 s and is automatically adjusted between

7   0.5 s and 60 s. Updated values of the saturation of structural reservoirs for each of the seven

8   layers and the depth of ponded water in the macro-crack are calculated according to the

9   volume of water that infiltrates into the matric porosity with respect to the source function S_w

10   or the Dirichlet boundary condition. Excess of water is then added at the surface of the soil

11   prism in structural porosity, and a new profile of saturation of each reservoir is calculated. At

12   least, the new vertical boundary condition for Richards' equation along the crack wall is

13   updated.

14   **3- Material and methods**

15   **3.1- Description of the experiments**

16   The model was tested on a Vertisol at the Experimental Research Station of INRA in Gardel,

17   Guadeloupe (French Antilles). The aim of the experiments was to give data to calibrate and

18   validate the model.

19   *Soil*

20   The soil is a chromic vertisol, with more than 80 % clay (< 2 µm). Main soil features are in

21   Appendix A1.1. The plot has been grown with Stargrass (*ynodon nemfluensis)* for more than

22   10 years. Macro-cracks open during the dry season along a large network delimiting prisms of

23   about 70 cm in width. The soil profile is described in Appendix A1.2.

24   *Experimental site (Figure 2)*

25   The network of macro-cracks was plotted at the end of the dry season. Several soil prisms

1 were isolated from the plot by a polyethylene sheet coated with a hull of resin and fibre-glass.

2 A side of the hull was replaced by a rigid inox steel-plate on which the measurement devices

3 were fixed. Then, the soil was excavated at the front of the inox steel-plate. Four windows

4 were cut into the inox sheet and equipped with Plexiglas plates. Water stored in macro-cracks

5 could be removed at different depths through holes made in one of the Plexiglas sheet.

6 *Soil movement measurements*

7 Potentiometric sensors (50 µm precision, Essor Français Electronique, Ivry la Bataille,

8 France) were fitted on the remaining Plexiglas windows to measure the horizontal

9 deformation of a soil prism at different depths: 7, 27, 47, 67, 87 cm, with three replicates per

10 depth. Data were collected on a Campbell CR21X data logger (Campbell Scientific,

11 Shepshed, UK) every 5 minutes. All the displacement sensors were installed on the same soil

12 prism.

13 Thickness variations of prism layers were measured with modified THERESA® transducers

14 (Cabidoche & Ozier-Lafontaine, 1995). The soil layers equipped were the 10-30 cm, 30-50

15 cm, 50-70 cm layers depth for the first set of transducers, and the 30-50 cm, 50-70 cm, 70-90

16 cm depth layers for the second set, with three replicates per set. Transducers were fitted with

17 the same potentiometric displacement sensors and data were collected on the CR21X data

18 logger every 5 minutes

19 *Water application*

20 For high rainfall intensities, water was applied at the soil surface with four full cone nozzles

21 (Lechler, Paris, France) fitted at the corners of a 1mx1m square frame. We used a portable

22 sprayer for low intensities. Homogeneity of rainfall was checked using five cans placed

23 randomly at the surface.

24 *Water content measurements*

25 In swelling soils, the water content cannot be measured by usual devices (neutron probe,

1   tensiometers, TDR, capacitance probes) because of soil movement. The matric WC was

2   calculated with the model of Voltz & Cabidoche (1995) from thickness variations of prism

3   layers measured with the modified THERESA® transducers. When using these transducers,

4   prism layers are define as layers containing a constant mass of solid particles (material

5   description). Therefore the volume of a prism layer is not constant and is related to the soil

6   matric water content. The model of Voltz & Cabidoche assumes that the shrinkage of a prism

7   layer is a normal shrinkage, i.e. that a decrease of the matric water content results in the same

8   decrease of the apparent prism layer volume. If the anisotropy of soil movements is known,

9   then the thickness variation of a prism layer can be converted into volume variation and then

10 converted into matric water content changes. The structural WC was not measured. A

11 piezometer was fitted into a macro-crack: the level of ponded water was automatically

12 measured by an ultrasonic probe and stored in a data logger (CR2M, France) every minute.

13 **3.2- Measurements of input parameters**

14 Two sets of parameters are required: one set to calculate the profile of the matric WC from

15 vertical thickness measurements, which in turn becomes the initial conditions of the model

16 (matric WC and crack aperture), the other set is directly used by the model. The method of

17 Cabidoche & Voltz (1995) was used to measure the first set of parameters, which are: the

18 specific volume of solids, the specific volume of air and the matric WC at the crack air entry

19 point. The second set of parameters (the water retention curve, the shrinkage curve, and the

20 matric hydraulic conductivity) was measured according to the methods described in Ruy &

21 Cabidoche (1998). The anisotropy ratio k was calculated from *in situ* measurements of vertical

22 and horizontal soil movements (Ruy, 1997).

23 **3.3- Sensitivity analysis**

24 Uncertainty exists at the level of all inputs of the model. We can distinguish between

25 parameters related to the geometry of the domain (anisotropy ratio k, diffusion length d, size

1   of the prism), those related to the water infiltration (matric hydraulic conductivity $K_{w/s}$,

2   anisotropy k, conductance c, exponent b, structural porosity, …) and those defining the initial

3   and boundary conditions (matric and structural WC, rainfall intensity, …). As it is almost

4   impossible to perform a multivariate sensitivity on all these parameters, we will focus on the

5   most relevant ones which are either the parameters that can't be measured and then should be

6   fitted (conductance c and diffusion length d) or the parameters that were measured with a high

7   experimental uncertainty (anisotropy k and structural porosity). Outputs of the model are the

8   cumulated flows into the three porosities ("matric flow", "structural flow" and "macro-crack

9   flow") and the cumulated runoff after 10000 sec of simulation. Cumulated matric flow is the

10   sum of the cumulated infiltration from the soil surface, the horizontal infiltration from the

11   macro-crack and the amount of water that flows from structural to matric porosity. Initial

12   values of the parameters used in the sensitivity analysis are 0.85 for k, 0.01 cm s^{-1} for c, 1 cm

13   for d and 0.437 dm^3 kg^{-1} for structural porosity. The range of variations is shown in Table 3.

14   The analysis is first a "one-at-a-time analysis" on the previous parameters that may reveal

15   some discontinuities of the model. Parameters are then gathered to account for correlation

16   between them in a qualitative way. Indeed, soil structure parameters (structural porosity,

17   conductance c, diffusion length d) may not be independent: if structural porosity is important

18   and well connected, then the size of aggregates decreases and c should increase and d should

19   decrease. However, it is not possible to calculate the correlation between them because c and

20   d can not be measured and they are essentially empirical. Three sets of parameters were used:

21   one set with the initial values (set #0), another one (set #1) with a "low" structural porosity,

22   the last one (set #2) with a "high" structural porosity (Table 3).

23   **3.4- Fitting of unknowns parameters**

24   Structural conductance c and diffusion length d must be fitted from experimental data. Both

25   parameters are soil structure parameters: they should vary with depth because the volume and

1   the shape of the structural pores vary with depth (Table 4). In the surface layer (0-50 cm)

2   structural pores are channels, packing pores and planar voids, whereas they are mainly

3   channels in depth. We considered two different values for c: c_{surf} (layers 0-10 cm and 10-30

4   cm) and c_{deep} (30-50 cm to 90-110 cm). c is nil at 130 cm, because of the impervious layer.

5   Three different values were considered for d: d_{surf} (0-10 cm, 10-30 cm, 30-50 cm), d_{mid} (50-70

6   cm, 70-90 cm) and d_{deep} (90-110 cm and 110-130 cm). Therefore 5 parameters must be fitted

7   from experiments. Exp1 to Exp5 provided data to calibrate the model from soil layer

8   thickness measurements. Let us denote $\mathbf{U}$ the vector of these parameters. $\mathbf{U}$ was determined by

9   minimising the least-squares objective function $SSE(\mathbf{U})$ using the Marquardt method (1963):

$$SSE(\mathbf{U}) = \sum_{i=1}^{4}\left(\sum_{j=1}^{T}\left(\bar{s}_i\left(t_j\right) - \hat{s}_i\left(t_j,\mathbf{U}\right)\right)^2\right) , \tag{3}$$

10   where i is the number of soil layers (from layer 1: 10-30 cm to layer 4: 70-90 cm depth), T the

11   total number of time intervals, t_j the time (sec), $\bar{s}_i\left(t_j\right)$ (cm) the mean swelling that is measured

12   on layer i, and $\hat{s}_i\left(t_j,\mathbf{U}\right)$ (cm) the mean swelling of layer i that is simulated by the model.

13   **4- Results**

14   **4.1- Submodels validation**

15   The model can be run in 3 domains, 2 domains (matric porosity + structural porosity or

16   macro-crack) or 1 domain (only matric porosity). When run in 1 domain, the model has been

17   successfully checked against experimental data obtained in two rigid porous media

18   (Haverkamp *et al.*, 1977) and in a 1D swelling bentonite paste (Angulo *et al.*, 1990; Figure 3).

19   We used the model in two domains (matric porosity and macro-cracks). A rainfall of 120 mm

20   h[-1] for 6 min was simulated (frequency 0.9 year^{-1} in the Grande-Terre island of Guadeloupe).

21   Figure 3 shows that most of the rain flows into the macro-crack where it accumulates and then

22   infiltrates into the soil prism, resulting in both horizontal and vertical swelling of the prism.

1   The pattern of the heterogeneity of water potentials inside the prism (Figure 4) is very similar

2   to the spatial variability of the water content measured in the field (see Figure 7 of Jaillard &

3   Cabidoche, 1984). Therefore, we consider that these quantitative and qualitative results

4   validate the model when run with 1 or 2 domains (matric porosity and macro-cracks).

5   **4.2- Experiments results**

6   Six independent experiments, called Exp1 to Exp6, were performed. Initial matric contents

7   and the application rate of water are shown in Table 5. Macro-crack flow has never been

8   observed, except in the last experiment. The mean vertical swelling of the prism layers for

9   Exp4 are shown in Figure 5. For each experiment, the variation in the swelling measured by

10   transducers is quite large. For example, we plotted data collected in the 30-50 cm layer during

11   Exp5 in Figure 6. Two assumptions can be made to explain this heterogeneity: (i) a

12   preferential flow of water along the axis of the transducer, (ii) a large variability of the

13   structural porosity inside the prism. The first hypothesis has to be rejected because such a flow

14   should be stopped by the first anchor of the transducer into the soil (at a depth of 10 cm or 30

15   cm depending on the set of transducers), and then could not be recorded by the lower

16   transducers. Therefore, only the horizontal heterogeneity of the structural porosity explains

17   this discrepancy between the transducer. This heterogeneity is not incorporated into the

18   model.

19   Variations in the level of water in macro-cracks for Exp6 is plotted in Figure 12, and the mean

20   swelling velocity of the 10-30cm layer is plotted in Figure 7. The swelling velocity increases

21   as the level of water into the macro-crack reaches the 10-30 cm layer. It shows that lateral

22   infiltration into the prism of water running rapidly downwards along cracks has to be

23   neglected and that it must be taken into account under the level of ponded water into the

24   macro-crack.

25   **4.3- Measurements of input parameters**

1 Parameters of the model of Voltz & Cabidoche (1995) are shown in Table 4. The shrinkage

2 curve, the water retention curve and the matric hydraulic conductivity are not shown in this

3 paper but are detailed in Ruy (1997). Two layers were considered: the surface layer (0-50 cm

4 in depth) and the deep layer (50-100 cm in depth). In the range of the *in situ* soil moisture, the

5 shrinkage was normal. Water retention curves for both layers were fitted with the Van-

6 Genuchten model (1980) (Table 4). *k* is equal to 0.826 m m^{-1} (Ruy, 1997).

7 **4.4- Sensitivity analysis**

8 *(i) one-at-a-time analysis*

9 Cumulated runoff is the most sensitive output of the model, but it is not important (a few

10 mm).

11 Only cumulated macro-crack flow and runoff are sensitive to *k*: increasing *k* results in

12 converting vertical swelling into horizontal movement, and therefore in closing the macro-

13 crack more quickly. The volume of the macro-crack decreases and runoff is enhanced.

14 Cumulated matric flow is highly sensitive to *d* (Figure 8), as the main component of

15 cumulated matric flow is the water diffusion from structural porosity and as the source

16 function S_w is inversely proportional to d^2 (*eq*. (1)). Indeed with the initial values of the

17 parameters, water balance inside the matric porosity shows that only 0.14 mm water infiltrates

18 from the soil surface, 1.1 mm from macro-cracks walls and 6.1 mm from the structural

19 porosity. As a consequence, swelling of the soil prism increases as *d* decreases and that results

20 in a decreasing volume of the macro-crack and therefore in an increase of runoff. We could

21 expect that increasing (resp. decreasing) *d* would decrease (resp. increase) the cumulated

22 structural flow as it decreases (resp. increases) the amount of water uptake from structural

23 porosity within matric porosity. However, *d* has no influence on the cumulated structural flow

24 as it is controlled by the infiltrability of the structural porosity, which is solely a function of

25 the conductance *c*.

1   All outputs of the model are sensitive to conductance c. As the infiltrability of the structural

2   porosity is a function of c, increasing c increases the velocity of structural water flow and

3   increases the amount of water infiltrating into structural porosity. Therefore, we obtain less

4   cumulated macro-crack flow and runoff (Table 3). However, cumulated matric flow is not

5   very sensitive to c within the range [0.005 cm s^{-1}; 0.01 cm s^{-1}]: inside these limits, water flow

6   from structural to matric porosity is governed by the diffusion length d. If c is lower than

7   0.005 cm s^{-1}, cumulated structural flow is very limited and the amount of water that may enter

8   into the matric porosity according to eq. (1) is decreased. If c is greater than 0.01 cm s^{-1}, water

9   infiltrates more quickly and deeper into the structural porosity: saturation S_{struc} of the upper

10   layers is decreased, and the amount of water that flows from structural to matric porosity

11   according to eq. (1) is also decreased.

12   The model is not very sensitive to the value of the structural porosity.

13   *(ii) sensitivity analysis on set of parameters (Table 3)*

14   For set #1, the variation of the cumulated matric flow is mainly explained by the decrease of

15   d, whereas the variation of c has an influence on cumulated structural and macro-crack flows,

16   and then on runoff. For set #2, the variation of d has little effects and concerns only cumulated

17   matric flow: increase of cumulated structural flow and disappearance of macro-crack flow and

18   runoff is explained by the increase of c and of the structural porosity.

19   As a conclusion, the model is not sensitive to k and to the value of structural porosity which

20   are both measured in the field. It is sensitive to the structural conductance c and to the

21   diffusion length d which are empirical soil structure parameters that must be fitted.

22   **4.5- Calibration**

23   Exp1 to Exp5 were used for calibration. During these experiments, we never observed water

24   flow into the macro-crack. Therefore, only 1D infiltration into the prism occurred. As swelling

25   of layers under the 90 cm depth was not recorded, d_{deep} was set to 4 cm.

1   First we checked the uniqueness of the parameters estimation using the data of Exp3. The

2   time of simulation was 4080 sec (68 min). Parameter estimations were conducted with three

3   different initial parameter sets. A fourth estimation was carried out with a time of simulation

4   of 10000 sec. Results are presented in Table A2.1. For all the parameters and estimations,

5   except for d_{mid}, the standard error of estimation is not high compared to the parameter value.

6   For d_{mid}, the standard error of estimation is at least 100 % of the value, except for estimation

7   #4 where the standard error decreases to 15 % of the value. This is explained by the fact that

8   the swelling of deep layers was delayed and occurred only after about 4000 sec. Final

9   parameter values are not very different from one simulation to another and confidence

10   intervals greatly overlap. This suggests that the fitted parameters are unique. This has been

11   confirmed by other investigations carried out by Ruy (1997). Measured and simulated

12   swelling of 10-30 cm depth and 50-70 cm depth soil layers after calibration (estimation #4) is

13   plotted against time in Figures 9a and 9b respectively, which shows a good agreement

14   between simulation and measurements.

15   Estimations of all parameters for Exp1 to Exp5 are presented in Table A2.2. The measured

16   swelling of all layers for Exp1 and Exp5 is plotted against the simulated swelling in Figures

17   10a and 10b respectively. d_{deep} was fitted only from Exp5, because the swelling of deep layers

18   was not large in the other experiments: its value was 2.62 cm. Values of d_{mid} are different

19   from one experiment to another but 95 % confidence intervals greatly overlap. Therefore, a

20   mean value could be estimated by a weighted average of the values per experiment, with the

21   weight inversely proportional to the estimation variances. The estimated average was 2.45 cm.

22   Fitted values of d_{surf} also differ from Exp1 to Exp5 and 95 % confidence intervals do not

23   overlap. As the size of aggregates is a function of the matric WC, we tried to relate d_{surf} to the

24   initial matric WC of the 10-30 cm layer, but the regression was not significant. Therefore, a

25   mean value was also estimated by a weighted average of the values per experiment, the

1   average value was 0.440 cm. Fitted values of d increase with depth. This result was expected

2   because structural porosity decreases with depth.

3   Fitted values of c_{surf} and c_{deep} differ from one experiment to another. They can be explained

4   neither by the initial matric WC, nor by rainfall intensity R. Germann & Di Pietro (1996)

5   distinguished two kinds of flow in macropores, *i.e.* dispersive and preferential flow. They

6   showed (see Table 3 of Germann & Di Pietro, 1996) that conductance is constant when water

7   infiltration is governed by preferential flow (for large input rates of water), and increases with

8   the rainfall intensity when the flow in macropores is dispersive (for low input rates). In our

9   experiments, low input rates of water in Exp2, Exp3 and at the beginning of Exp4 could be

10   responsible for a dispersive infiltration, whereas the second part of Exp4 and Exp5 could have

11   been governed by preferential flow. However, this result cannot explain the difference

12   between Exp2 and Exp3 where rainfall intensities are the same. In fact, other factors, such as

13   geometry and initial saturation of structural porosity, have an influence upon the value of

14   structural conductance.

15   **4.6- Validation**

16   Finally, we tested the model with the independent data set collected during Exp6. Parameter

17   values used in the simulation are 0.440 cm for d_{surf}, 2.45 cm for d_{mid}, 2.62 cm for d_{deep}, 0.0434

18   cm s^{-1} for c_{surf} and 0.0478 cm s^{-1} for c_{deep}. Values of c_{surf} and c_{deep} are those fitted in Exp5

19   because rainfall intensities of Exp5 and Exp6 are close.

20   Simulation results are presented in Figures 11 and 12. Neither the range of swelling nor its

21   rate are simulated in a satisfactory way. For deep layers, however, simulated swelling is inside

22   the 68 % confidence interval (Figure 11b). The worst simulations are obtained for the layer

23   30-50 cm (Figure 11a). No swelling is simulated by the model at the beginning of the water

24   input. Matric conductivity is very low (2×10^{-6} cm day^{-1}) because of the low initial matric WC.

25   Therefore, the amount of water that moves from structural to matric porosity is almost nil. The

1 rapid swelling that occurs after about 4000 sec is due to the upraising of the saturation in

2 structural porosity. The model simulates the closure of the macro-crack at the surface after

3 6000 sec: this was not observed in the field and the swelling is recorded for 10000 sec more.

4 Simulated time variations of the level of ponded water in the macro-crack are different from

5 measurements (Figure 12). Water flow in the macro-crack is recorded for 2520 sec (42 min)

6 after the beginning of the rainfall, whereas it is simulated after 6120 sec (102 min). The

7 beginning of water infiltration into the macro-crack is delayed by the model, because of the

8 high infiltrability of the structural porosity (structural conductance of 0.0434 cm s^{-1} at the

9 surface). However, the upraising of the water level is well simulated: measurements (resp.

10 simulation) show that water reaches the level of 120 cm 720 sec (resp. 600 sec) after the

11 beginning of the flow in the macro-crack. After rainfall has stopped, the decrease of the water

12 level in the macro-crack is not well simulated. However, at least two reasons can explain this

13 discrepancy. (i) clogging of the piezometer by deposit of clay particles: therefore, the level

14 recorded inside the piezometer is higher than the water level in the macro-crack; (ii) artefacts

15 of simulation: as the macro-crack closes up, a small variation in the amount of water in the

16 macro-crack results in a large variation in the level of water.

17 **5- Discussion**

18 **5.1 Physical representativeness of the model**

19 Macro-crack flow, matric flow and soil deformation have been validated (**section 4.1**). Two

20 components of the model can be questioned: (i) rainfall partition at the soil surface between

21 matric and structural porosity, and (ii) modelling of water flow in the structural porosity.

22 Besides the modelling of rainfall partition that we used is widely used (e.g. Jarvis & Leeds-

23 Harrison, 1987; Jarvis 1994), it is true only for infiltration saturating pores of increasing size.

24 In our case, (i) matric flow is a saturating infiltration and (ii) the model simulates

25 simultaneous infiltration in both matric and structural porosities as the computed matric

1   infiltrability is very low. Therefore the conditions of validity of the hypothesis about rainfall

2   partition are met and there is no reason to change this module.

3   **5.2 Is water flow in structural pores preferential and turbulent ?**

4   Flow can be laminar or turbulent depending on the value of the dimensionless Reynolds

5   number, *Re*. *Re*=2000 is the limit between the two kinds of flow for open channel flow or pipe

6   flow. Usually, the limit is between 1 and 10 in porous media (Chen & Wagenet, 1992), which

7   corresponds to a pore diameter of about 100 µm. Moreover, theoretical values of *b* are related

8   to the flow conditions. *b* is equal to 2 (resp. 3) for a laminar flow in a smooth and vertical

9   plane pore (resp. a smooth and vertical tubular pore) and is between 2/3 and 5/3 for a

10   turbulent flow. Germann & Di Pietro (1996) analysed results obtained on drainage

11   hydrographs. They showed that gravity-dominated flow can be either of the preferential type

12   or of the dispersive type: in their experiments, the value of *b* was not constant but may be used

13   to assess the degree of preferential flow. *b* decreased with increasing application rates of

14   water. Its value was about 4 for a preferential flow (application rate of water equal to about

15   360 mm h^{-1}), and increased up to 8 for a more dispersive flow (application rate of about 36

16   mm h^{-1}). According to these authors, the power law relation between the flux and the

17   saturation is the same as the power law relation between the hydraulic conductivity and the

18   saturation for a fully dispersive flow. In this case, the conductance is the hydraulic

19   conductivity at saturation, and *b* ranges from 11 to 30 (Clapp & Hornberger, 1978).

20   Therefore, there is no reason to set *b* at a constant value of 1.5 for all our experiments. Indeed,

21   (i) the range of the application rates of water at the soil surface (Table 5) indicates that the

22   type of flow could change from dispersive to preferential, and (ii) the range of structural pore

23   sizes in the soil (10 µm to several mm, Ruy, 1997) indicates that flow conditions could change

24   from turbulent to laminar flow. New calibration could be conducted with *b* as an unknown

25   parameter. However, the total number of parameters would increase and parameters *b* and *c*

1 would probably not be independent.

2 **5.3 Is water flow in structural pores really preferential ?**

3 Hypothesis that structural flow is of preferential type came from the results of Ruy (1997).

4 However, the experimental uncertainty in the calculation of structural and matric WC was

5 quite important. It is possible that Darcy's law may be applied on one part of the structural

6 flow (in the smallest pores) and that a gravity-dominated flow may be used for the other part

7 of the structural flow, as the range of variation of the pore diameters is quite large. We used

8 the Wind's evaporation method (Tamari *et al.*, 1993) to obtain the hydraulic conductivity of

9 the structural porosity ("structural conductivity") on one saturated clod sampled in the 70-80

10 cm layer. Results are only approached as the shrinkage is not accounted for in this method, but

11 we see (Figure 13) a good agreement between the matric conductivity and the structural

12 conductivity, showing that Darcy's law could be used at least in one part of the structural

13 porosity.

14 **6- Conclusion**

15 We presented a mechanistic model of water infiltration in a *in situ* Vertisol of Guadeloupe.

16 that required some calibration. It is possible to find a unique set of parameters for each

17 experiment. However, parameters significantly differ from one experiment to another.

18 Therefore, the model is not fully validated. This is due to a poor modelling of water flow in

19 the structural porosity. Nevertheless, our model already shows that infiltration in this soil is a

20 3D process and that the structural water flow is the main factor of the partition of water

21 between vertical infiltration in the prism and water flow in macro-cracks. Unfortunately, the

22 measurement of this process is impossible in the field. In fact, we don't know if structural flow

23 is preferential or if Darcy's law could be used. More researches are therefore needed to better

24 understand the processes of water infiltration in the structural porosity.

25 **Acknowledgements**

References

Angulo, R., Gaudet, J.P., Thony, J.L. and Vauclin, M., 1990. Conductivité hydraulique d'un milieu poreux partiellement saturé, déformable. II. Résultats expérimentaux. Comptes Rendus de l'Académie des Sciences de Paris, série II, 310, 341-345.

Beven, K. and German, P., 1981. Water flow in soil macropores. II. A combined flow model. Journal of Soil Science, 32, 15-29.

Beven, K. and German, P., 1982. Macropores and water flow in soils. Water Resources Research, 18, 1311-1325.

Bronswijk, J.J.B., 1988. Modeling of water balance, cracking and subsidence of clay soils. Journal of Hydrology, 97, 199-212.

Cabidoche, Y.M. and Ozier-Lafontaine, H., 1995. THERESA: I. Matric water content measurements through thickness variations in vertisols. Agricultural Water Management, 28, 133-147.

Cabidoche, Y.M. and Voltz, M., 1995. Non-uniform volume and water content changes in swelling clay soil: II. A field study on a Vertisol. European Journal of Soil Science, 46, 345-355.

Chen, C. and Wagenet, R.J., 1992. Simulation of water and chemicals in macropore soils. Part 1. Representation of the equivalent macropore influence and its effect on soil water flow. Journal of Hydrology, 130, 105-126.

Clapp, R.B. and Hornberger, GM, 1978. Empirical equations for some soil hydraulic properties. Water Resources Research, 14, 601-604.

Di Pietro, L., 1996. Application of a lattice-gas numerical algorithm to modelling water transport in fractured porous media. Transport in Porous Media, 22, 307-325.

Durner, W., 1994. Hydraulic conductivity estimation for soils with heterogeneous pore structure. Water Resources Research, 30, 211-223.

Garnier, P., Perrier, E., Angulo Jaramillo, R. and Baveye, P., 1997. Numerical model of 3-dimensional anisotropic deformation and 1-dimensional water flow in swelling soils. Soil Science, 162, 410-420.

Germann, P.F. and Di Pietro, L., 1996. When is porous media flow preferential? A hydromechanical perspective. Geoderma, 74, 1-21.

Haverkamp, R., Vauclin, M., Touma, J., Wierenga, P.J. and G. Vachaud, 1977. A comparison of numerical simulation models for one-dimensional infiltration. Soil Science Society of America Journal, 41, 285-294.

Hoogmoed, W.D. and Bouma, J., 1980. A simulation model for predicting infiltration into cracked clay soil. Soil Science Society of America Journal, 44, 458-461.

Jaillard, B. and Cabidoche, Y.M., 1984. Etude de la dynamique de l'eau dans un sol argileux gonflant: dynamique hydrique. Science du sol, 22, 239-251.

Jarvis, N.J., 1994. The MACRO model (version 3.1): technical description and samples simulations. Reports and Dissertations No 19, Swedish University of Agricultural Sciences, Uppsala.

Jarvis, N.J. and Leeds-Harrison, P.B., 1987. Modelling water movement in drained clay soil. I. Description of the model, sample output and sensitivity analysis. Journal of Soil Science,38, 487-498.

Maheshwari, B.L., 1994. Values for the exponent of the storage-discharge equation in runoff-routing models. Journal of Hydrology, 163, 95-106.

Marquardt, D.W., 1963. An algorithm for least squares estimation on non-linear parameters. Journal of the Society for Industrial and Applied Mathematics, 11, 431-441.

Philip, J.R., 1969. Hydrostatics and hydrodynamics in swelling soils. Water Resources Research, 5, 1070-1077.

Ruy, S., 1997. Les trois voies simultanées de l'infiltration dans un vertisol de Guadeloupe: études expérimentale et numérique. PhD. thesis, University of Montpellier II, Montpellier.

Ruy, S. and Cabidoche, Y.M., 1998. Hydraulic conductivity of the matric porosity of an unsaturated Vertisol: a field and laboratory comparison. European Journal of Soil Science, 49, 175-185.

Stirk, G.B., 1954. Some aspects of soil shrinkage and the effect of cracking upon water entry into the soil. Australian Journal of Agricultural Research, 5, 279-290.

Tamari, S., Bruckler, L., Halbertsma, J. and Chadoeuf, J., 1993. A simple method for determining soil hydraulic properties in the laboratory. Soil Science Society of America Journal, 57, 642-651.

Van Genuchten, M.T., 1980. A closed-form equation for predicting the hydraulic conductivity of unsaturated soils. Soil Science Society of America Journal, 44, 892-898.

Voltz, M. and Cabidoche, Y.M., 1995. Non-uniform volume and water content changes in

1   swelling clay soil: I. Theoretical analysis. European Journal of Soil Science, 46, 333-343.

2   Wilding, L.P. and Tessier, D., 1988. Genesis of vertisols: shrink-swell phenomena. In: L.P.

3   Wilding and R. Puentes (Editors), Vertisols: their distribution, properties, classification and

4   Management, Texas A&M University Printing Centre, College Station TX, 55-81.

5   Yule, D.F. and J.T. Ritchie, 1980. Soil shrinkage relationships of Texas vertisols: II. Large

6   cores. Soil Science Society of America Journal, 44, 1285-1291.

Appendix 1: soil description at the experimental site

Appendix 2: calibration results

List of tables

Table 1: boundary condition for water flow at the soil surface. R is the rainfall intensity (cm s^{-1}), q^{in} (cm s^{-1}) the flux of water entering the matric porosity (subscript mat), the structural porosity (subscript struc) and the macro-crack (subscript crac). I^{max} (cm s^{-1}) is the infiltration capacity of the matrix, the structural porosity and the macro-crack, depending on the subscript.

Table 2: theoretical modelling of water flow in and between the three domains.

Table 3: sensitivity of model predictions of the amount of water stored in the matric porosity, the structural porosity, the macro-crack and the cumulated runoff to changes in input parameters. Initial values of parameters are: $k=0.85$, $c=0.01$ cm s^{-1}, $d=1$ cm (set #0). For set #1 (resp. set #2), structural porosity is decreased (resp. increased) by 10 %, c is divided (resp. multiplied) by 2 and d is increased (resp. decreased) by 10 %.

Table 4: parameters of the model of Voltz & Cabidoche (1995) relating thickness variations to the matric water content. θ_s, θ_r, α and n are the parameters of the model of Van Genuchten fitted to the retention curve: $\dfrac{\theta - \theta_r}{\theta_s - \theta_r} = \dfrac{1}{\left\{1 + \left(\alpha \cdot |\psi|\right)^n\right\}^{1 - 1/n}}$, where ψ is the matric potential (cm).

a and b are the coefficients of the logarithmic regression between the matric conductivity $K_{w/s}$ (cm day^{-1}) and the matric potential ψ (cm): $\log K_{w/s} = a + b \cdot \log|\psi|$.

Table 5: rainfall intensities and initial matric water content in the different experiments.

Table A1.1: soil characteristics at the experimental site (depth: 40-50 cm).

Table A1.2: soil profile at the experimental site.

Table A2.1: final parameters obtained from experiment Exp3.

Table A2.2: estimated parameters from all the experiments.

List of figures

Figure 11: variation of the measured and simulated swelling of the (11a) 30-50 cm and (11b) 70-90 cm depth layers during Exp6. Continuous lines are for the 60 % confidence interval.

Figure 12: variation of the measured and simulated water level in macro-cracks during Exp6.

Figure 13: hydraulic conductivity $K_{w/s}$ of the matric porosity and of the structural porosity of the 70-80 cm depth layer. θ is the volumetric water content (m^3 m^{-3}).

Table1

Rainfall intensity R			q_{mat}^{in}	q_{struc}^{int}	q_{crac}^{in}	Runoff
$R \le I_{mat}^{max}$			R	0	0	0
$R > I_{mat}^{max}$	$R \le I_{mat}^{max} + I_{struc}^{max}$		I_{mat}^{max}	$R - I_{mat}^{max}$	0	0
	$R > I_{mat}^{max} + I_{struc}^{max}$	$R \le I_{mat}^{max} + I_{struc}^{max} + I_{crac}^{max}$	I_{mat}^{max}	I_{struc}^{max}	$R - I_{mat}^{max} - I_{struc}^{max}$	0
		$R > I_{mat}^{max} + I_{struc}^{max} + I_{crac}^{max}$	I_{mat}^{max}	I_{struc}^{max}	I_{crac}^{max}	$R - I_{mat}^{max} - I_{struc}^{max} - I_{crac}^{max}$

Table 2

porosity	Equations		
	law of motion	mass balance	water exchanges:
matric	Darcy's law : $\mathbf{q}_{\mathrm{mat}} = -K_{\mathrm{w/s}}(\psi) \cdot \vec{\nabla}(\psi + z)$ 2D	Richards' equation: $C(\psi) \cdot \dfrac{\partial \psi}{\partial t} = \dfrac{\partial}{\partial x}\left(K_{\mathrm{w/s}}(\psi) \cdot \dfrac{\partial \psi}{\partial x}\right) + \dfrac{\partial}{\partial z}\left(K_{\mathrm{w/s}}(\psi) \cdot \left(\dfrac{\partial \psi}{\partial z}+1\right)\right) + S_w$	$S_w = K_{w/s}(\psi) \cdot S_{\mathrm{struc}} \cdot \dfrac{\psi_{\mathrm{struc}} - \psi}{d^2}$, $\psi_{\mathrm{struc}} = \psi^{ae} \cdot (1 - S_{\mathrm{struc}})$
structural	Gravity flow across 7 reservoirs: $q_{struc} = c \cdot S_{struc}{}^{b}, b = 1.5,$ 1D	for the ith reservoir : $\forall i \in [1..7], V_{\mathrm{max},i}\dfrac{dS_{\mathrm{struc},i}}{dt} = (q_{i-1} - q_i) - \int_i S_w(\theta_{mat}, S_{\mathrm{struc},i}, z)$	
crack	instantaneously added at the bottom of the macro-crack,	variation of the depth z^{SL} of the surface of the ponded water according to: **(i)** the flux of water at the surface of the macro-crack, **(ii)** the volume of ponded water that infiltrates horizontally into the soil prism, **(iii)** the swelling of the soil prism,	macro-crack - matric porosity: below the surface of ponded water, Dirichlet boundary condition: $\psi(z \le z^{SL}) = z^{SL} - z$, macro-crack - structural porosity: no exchange

Parameters		
matric porosity	hydraulic conductivity $K_{\mathrm{w/s}}(\psi)$ retention curve $\psi(\theta)$ shrinkage curve	measured measured measured
structural porosity	c d b ψ^{ae}	unknown: to fit unknown: to fit 1.5 measured: -316 cm

Table 3

parameter		% variation input	% variation output: amount of water stored into:			
			matric porosity	structural porosity	macro-crack	runoff
	0.7	-18	-0	0	-6	+15
	0.765	-10	-0	0	-3	+8
k (-)	0.85	0	0	0	0	0
	0.935	10	0	0	+3	-7
	1	18	0	0	+5	-11
	0.001	-50	-35	-73	+32	+1849
	0.005	-15	-3	-39	+7	+1028
	0.0075	-6	0	-19	+4	+502
$c^{\S}$	0.01	0	0	0	0	0
(cm s^{-1})	0.0175	12	-26	+13	-100	-100
	0.025	20	-37	+13	-100	-100
	0.05	35	-53	+13	-100	-100
	0.1	50	-59	+13	-100	-100
	0.25	-75	+111	0	-100	+232
	0.5	-50	+95	+1	-79	+148
	0.9	-10	+15	0	-12	+18
d (cm)	1	0	0	0	0	0
	1.1	10	-12	0	+10	-15
	1.5	50	-39	-1	+34	-56
	2	100	-57	-1	+44	-72
structural	0.393	-10	+1	-4	0	+118
porosity	0.437	0	0	0	0	0
(dm^3 kg^{-1})	0.481	+10	-1	+4	-2	-100
set #1			-15	-43	+17	+1103
set #0			0	0	0	0
set #2			-23	+13	-100	-100

§: % of variation of input c is % variation of |log(c)|

Table 4

layer	W^{ae}	v_a^{ae}	v_s	θ_s	θ_r	α	n	a	b
(cm)	(kg kg^{-1})	(dm^3 kg^{-1})	(dm^3 kg^{-1})	(m^3 m^{-3})	(m^3 m^{-3})	(cm^{-1})	(-)		
0-10	0.554	0.084	0.382						
10-30	0.534	0.080	0.379	0.6516	0.1141	0.1407	1.0468	-0.2328	-1.0926
30-50	0.508	0.075	0.373						
50-70	0.482	0.071	0.370						
70-90	0.456	0.066	0.370	0.6375	0.3675	0.1316	1.0801	-0.3141	-1.1718
90-110	0.430	0.061	0.370						

exponent ae is the crack air-entry point, W the matric water content, v_a the specific volume of air, v_s the specific volume of solid.

Table 5

Experiment	Date	Applied water			Initial matric water content $(kg\ kg^{-1})$			
		intensity $(mm\ h^{-1})$	time (min)	amount (mm)	layer 10-30 cm	layer 30-50 cm	layer 50-70 cm	layer 70-90 cm
Exp1	15/10/96	108.3	6	10.83	0.493	0.454	0.462	0.449
Exp2[*]	21/10/96	14.05	65	15.22	0.501	0.452	0.462	0.449
Exp3	24/10/96	14.43	60	14.43	0.524	0.456	0.462	0.449
Exp4	28/11/96	14.55	73	17.70	0.468	0.424	0.458	0.452
		62.12	13	13.46				
Exp5	12/12/96	72.31	53	63.87	0.490	0.433	0.460	0.452
Exp6	28/05/97	54.50	240	162.8	0.433	0.360	0.432	0.449

4 * partial loss of data

5

1   Appendix 1: Table A1.1

granulometry (fraction < 2mm)			Organic Carbon and Organic Matter		Exchangeable Cations				
$(10^{-2}$ kg·kg$^{-1})$			$(10^{-3}$ kg·kg$^{-1})$		$(10^{-2}$ mol kg$^{-1})$				
< 2µm	2-50 µm	50-2000 µm	OC	OM	CEC	Ca^{2+}	Mg^{2+}	Na$^+$	K$^+$
81	12	7	21.4	36.9	46.0	62.9	8.4	3.2	6.0

2   INRA-Gardel, n=2.

3

4

1   Appendix 1: Table A1.2

Layer (cm)	Colour	Structure
0-20	Black	Centimetric nuciform structure deriving from earthworm casts
20-40	Brownish black	From nuciform to centimetric polyhedral subangular structure
40-50	Greyish yellow brown	Large polyhedral structure with some slickensides
50-140	Yellowish brown	Wide oblique slickensides forming an "edge-shape" structure

2

3

4

Appendix 2: Table A2.1

Estimation	c_{surf} /cm s^{-1}		c_{deep} /cm s^{-1}		d_{surf} /cm		d_{mid} /cm	
	initial	final $(\sigma)^{\S}$	initial	Final $(\sigma)^{\S}$	initial	final $(\sigma)^{\S}$	initial	final $(\sigma)^{\S}$
1	0.02	0.0303 (0.0055)	0.005	0.0210 (0.0070)	1	0.5143 (0.0220)	1.5	4.69 (5.00)
2	0.03	0.0303 (0.0055)	0.02	0.0210 (0.0070)	0.5	0.5143 (0.0220)	4.5	4.68 (5.00)
3	0.01	0.0306 (0.0055)	0.0005	0.0213 (0.0075)	0.7	0.5117 (0.0225)	2.0	8.71 (17.0)
4[#]	0.025	0.0360 (0.0025)	0.01	0.0195 (0.0020)	0.55	0.5240 (0.0150)	3.0	1.31 (0.19)

2   [§]: σ is the standard error of the estimation of the parameter value (linear hypotheses).

3   [#]: for estimation #4, the time of simulation was 10000 sec instead of 4080 sec for the others.

4

Appendix 2: Table A2.2

experiment	c_{surf} $(\sigma^{\S})$	c_{deep} $(\sigma^{\S})$	d_{surf} $(\sigma^{\S})$	d_{mid} $(\sigma^{\S})$	d_{deep} $(\sigma^{\S})$
	/cm s^{-1}	/cm s^{-1}	/cm	/cm	/cm
Exp1	0.05	5.0	0.27	0.3	4
	(?)	(?)	(?)	(?)	
Exp2	0.0218	2.940	0.276	0.826	4
	(0.004)	(2.625)	(0.005)	(1.32)	
Exp3	0.0360	0.0195	0.524	1.31	4
	(0.0025)	(0.0020)	(0.015)	(0.19)	
Exp4	0.0395	0.725	0.293	39.14	4
	(0.008)	(0.223)	(0.02)	(460)	
Exp5	0.0420	0.0485	0.449	2.454	4
	(0.007)	(0.010)	(0.003)	(0.49)	
Exp5$^{\#}$	0.0434	0.0478	0.440	2.450	2.62
	(0.007)	(0.009)	(0.003)	(0.53)	(7.5)

2   §: σ is the standard error of the estimation of the parameter value (linear hypotheses).

3    $^{\#}$: the five parameters have been estimated.

4
5

1

Figure 1

Figure 2

soil layer thickness transducer

soil prism

piezometer

inox sheet

Plexiglas windows

○ holes draining the water
out of the macro-crack

● potentiometric
displacement sensors

⬤ position
of transducers
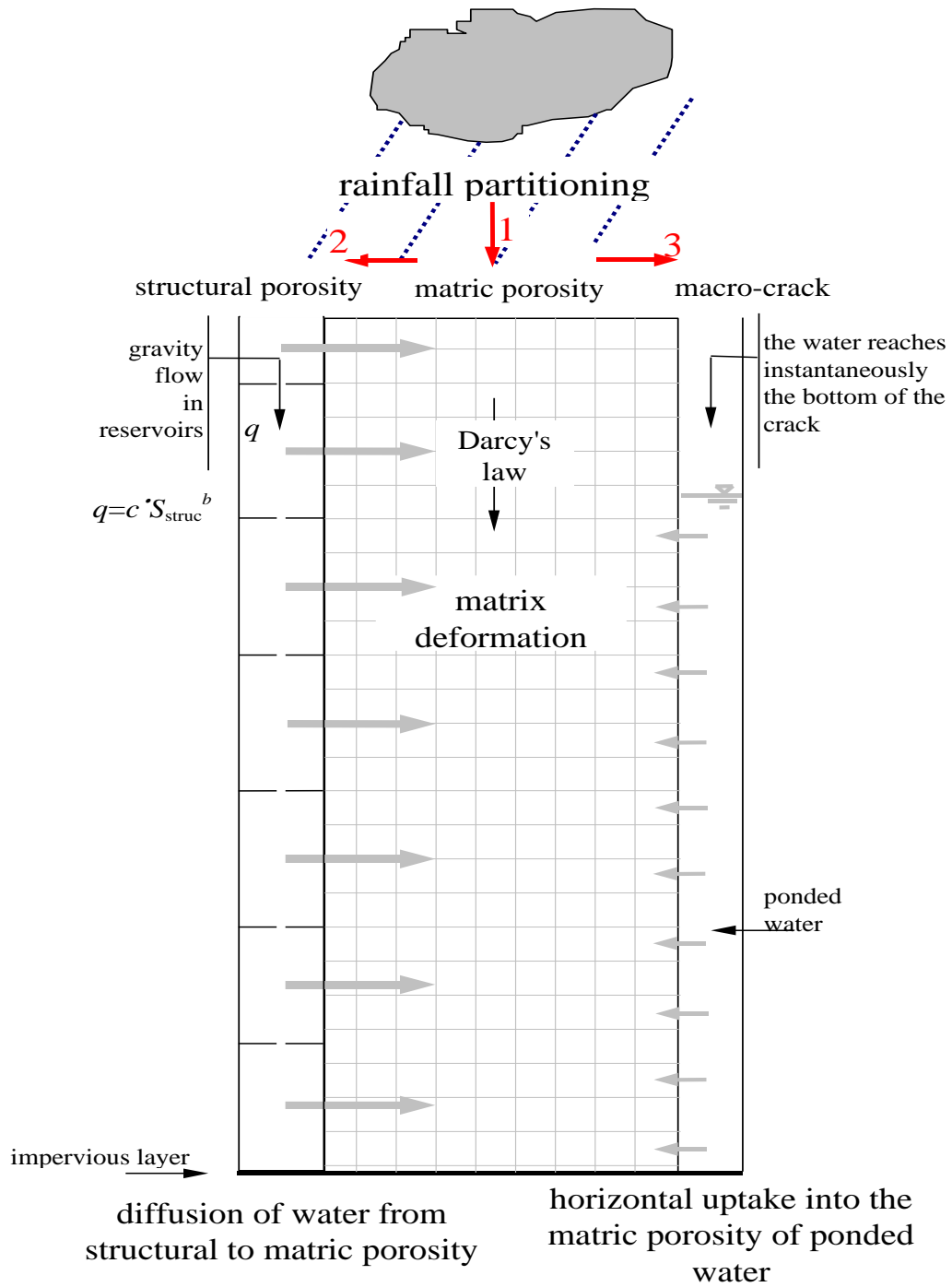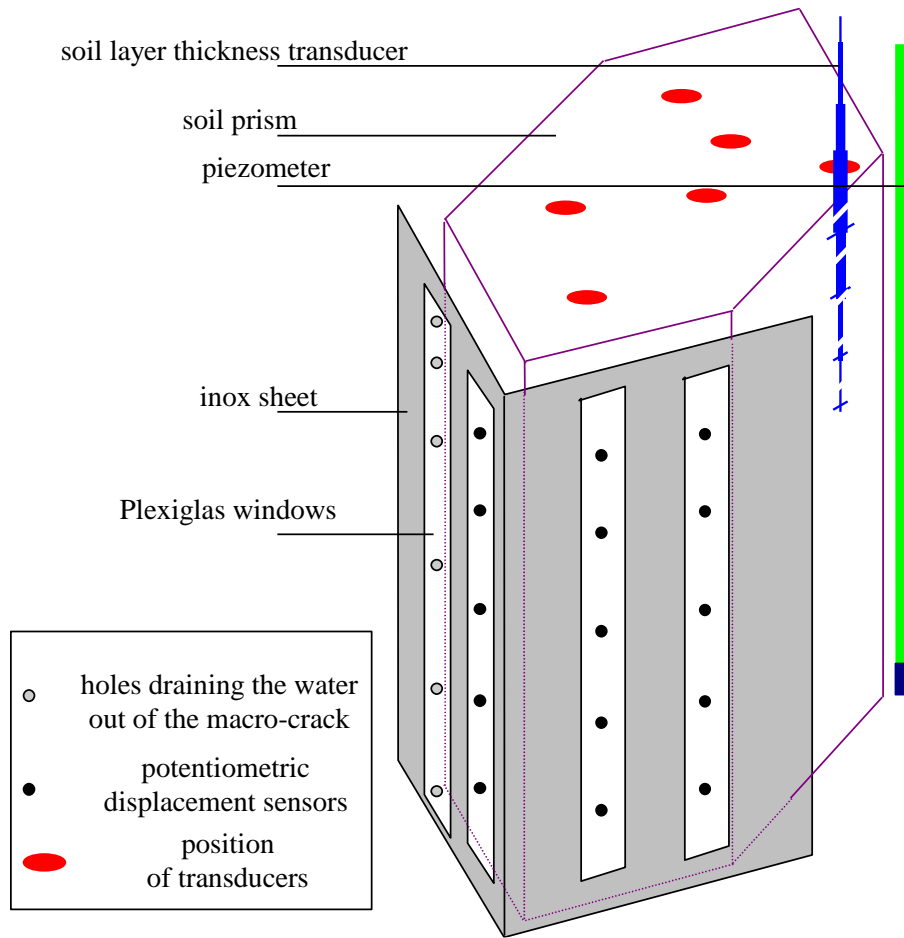
3

4

5

6
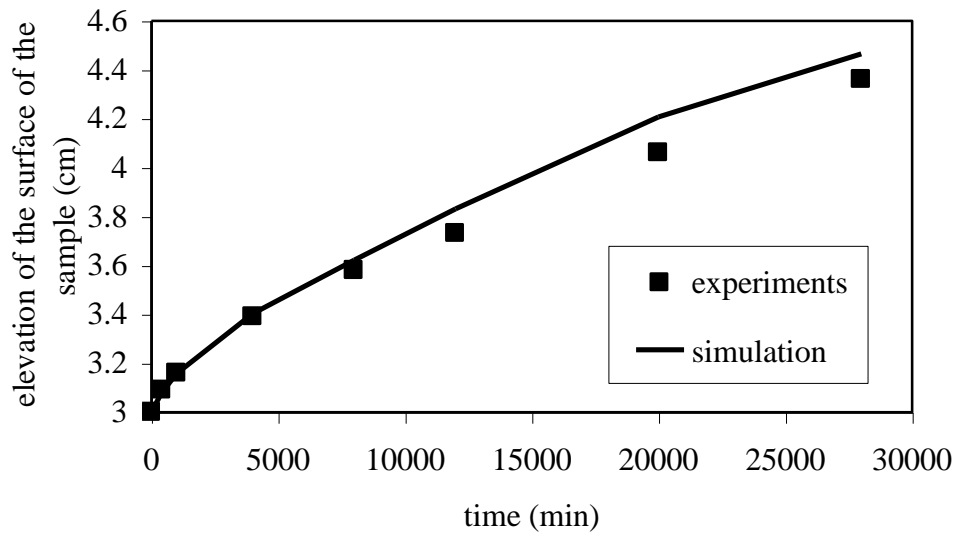
1   Figure 3

2

3   Figure 3a

4

5

6

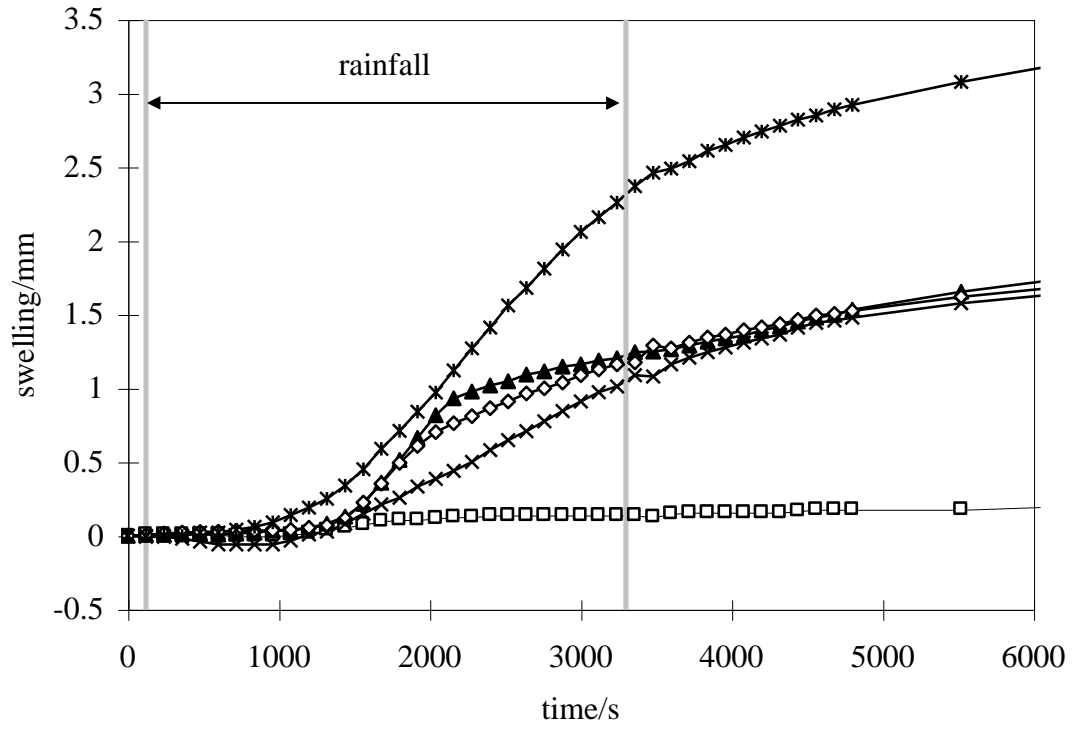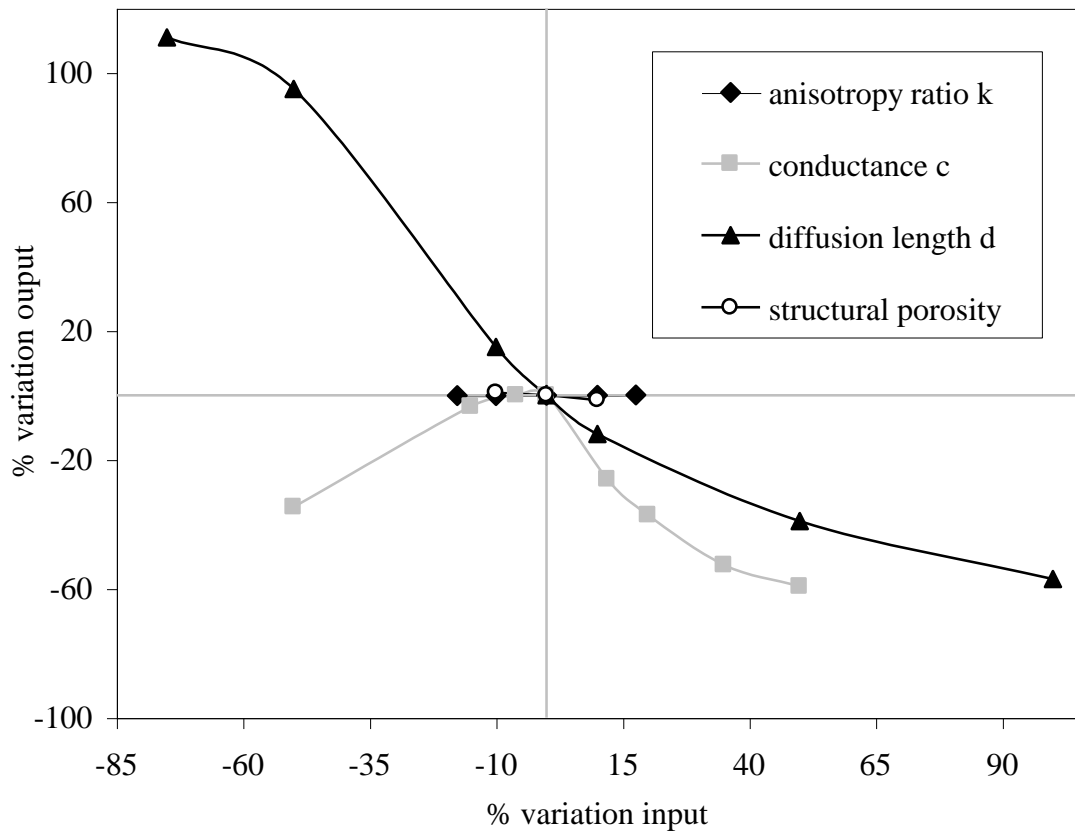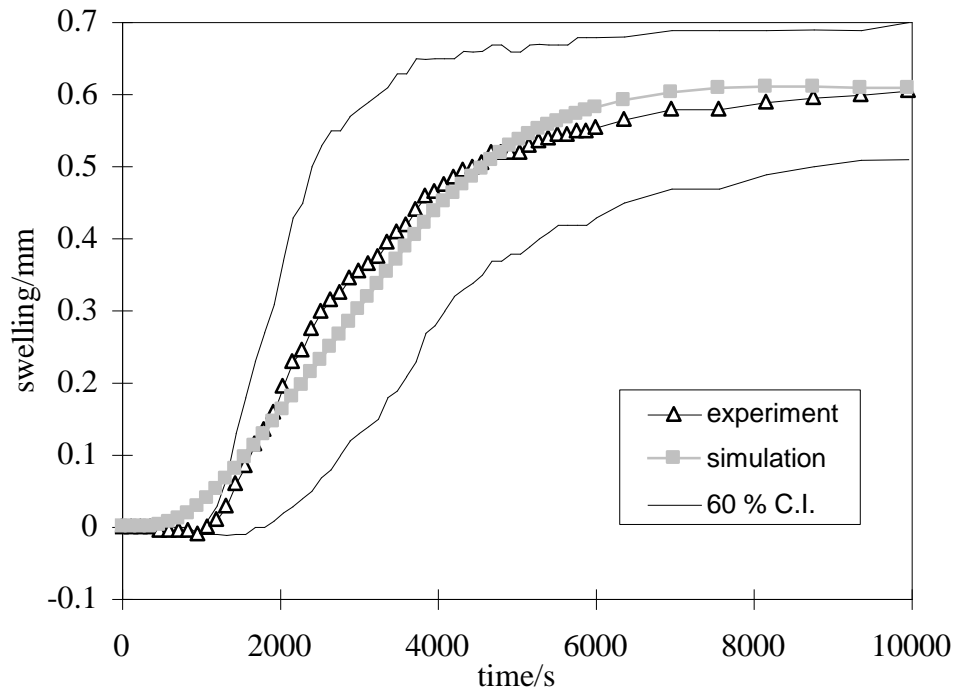7   Figure 3b

8

1

Figure 4

T = 6 mn   T = 1h30mn   T = 6h

potentials (cm)
-1000
-800
-700
-600
-300
-200
-100

depth (cm)

Distance / axis (cm)

crack

T=0   T=6 min   T=1h30min   T=6h

2

3

4

1

Figure 5

2

3
4
5

1

Figure 6

2

3

4

5

1   Figure 7

2

3

4

5

1

Figure 8

2
3

4
5

6

1   Figure 9

Figure 9a

2
3
4
5
6
7

8
9

10   Figure 9b

11
12

1

Figure 10

Figure 10a

Figure 10b

2
3
4
5
6

7
8
9
10

1   Figure 11

Figure 11a

2
3
4   Figure 11a
5
6
7
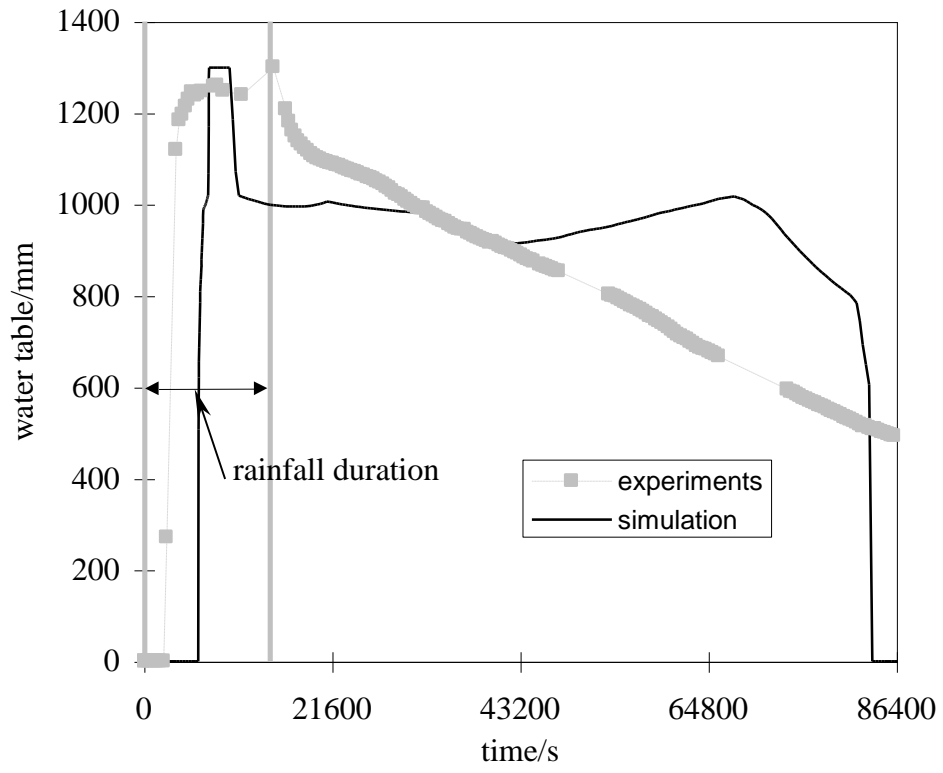

8
9
10   Figure 11b
11

45

1

Figure 12

2

3

Figure 13